Frontiers of Optoelectronics (2023) 16:6
https://doi.org/10.1007/s12200-023-00061-8

Frontiers of Optoelectronics

RESEARCH ARTICLE

Integrated contra-directionally coupled chirped Bragg grating waveguide with a linear group delay spectrum

Xudong Gao[1] · Zhenzhu Xu[1] · Yupeng Zhu[1] · Chengkun Yang[1] · Shoubao Han[1] · Zongming Duan[1] · Fan Zhang[2] · Jianji Dong[2]

Received: 2 December 2022 / Accepted: 27 February 2023

Abstract
Due to the advantages of low propagation loss, wide operation bandwidth, continuous delay tuning, fast tuning speed, and compact footprints, chirped Bragg grating waveguide has great application potential in wideband phased array beamforming systems. However, the disadvantage of large group delay error hinders their practical applications. The nonlinear group delay spectrum is one of the main factors causing large group delay errors. To solve this problem, waveguides with nonlinear gradient widths are adopted in this study to compensate for the nonlinear effect of the grating apodization on the mode effective index. As a result, a linear group delay spectrum is obtained in the experiment, and the group delay error is halved.

Keywords Bragg gratings · Silicon photonics · True time delay

1 Introduction

Phased array technology has important applications in radar and electronic countermeasure systems. At present, phased array radar is developing toward the use of higher frequency and wider bandwidth, but the bottleneck restricting its broadband characteristics comes from wideband phased array beamforming systems. In the traditional phased array system based on phase shifters, beam dispersion occurs in the wideband operation mode owing to the correlation between phase and frequency. In contrast, phased array systems based on true time delay can achieve broadband beamforming because the time delay is frequency-independent [1]. True time delay can be achieved by means of electric delay or microwave photonic delay. The electric delay chip has been widely used in phased array beamforming systems [2]; however, in the case of ultra-wideband, the crosstalk is serious owing to the high return loss, resulting in a large group delay error (GDE). Microwave photonic delay can be realized by electro-optic modulation, optical time delay, and photoelectric demodulation [3, 4]. Because photonic devices generally exhibit low return loss, the GDE of microwave photonic delay is expected to be small. Furthermore, it is potential to realize a microwave photonic delay system on a chip through hybrid integration techniques, as the integrated high-bandwidth electro-optic modulators [5, 6] and detectors [7, 8] have already been demonstrated in recent years. Therefore, integrated optical true time delay lines have recently attracted extensive research interest.

Integrated optical true time delay lines can be implemented using various approaches such as switches, optical ring resonators (ORRs), photonic crystal waveguides (PhCWs), and chirped Bragg grating waveguides. In switch-based delay lines, discrete delays can be realized by connecting switches with waveguides of different lengths and the time delay can be tuned by changing the switching state [1, 9, 10]. This method can achieve accurate delay, but the difficulty lies in the calibration of switches. Recently, calibration-free Mach–Zehnder switches have been implemented by introducing novel tapered Euler S-bends with a wide core and incorporating bent asymmetric directional coupler mode filters, paving the way toward the real application of switch-based delay lines [11]. ORRs have the advantages of continuous delay tuning and compact footprints. However, the operation bandwidth is limited by the delay-bandwidth

✉ Zhenzhu Xu
zhenzhupearl@163.com

[1] Anhui Province Engineering Laboratory for Antennas and Microwave, East China Research Institute of Electronic Engineering, Hefei 230000, China

[2] Wuhan National Laboratory for Optoelectronics, Huazhong University of Science and Technology, Wuhan 430074, China

Published online: 10 April 2023

product of a single ORR. To obtain a large delay with wide operation bandwidth, cascaded ORRs have been proposed. However, the tuning of cascaded ORRs become more difficult as well [12, 13]. PhCWs have a compact footprint owing to their strong optical confinement and slow-light effect [14, 15]. One-dimensional fishbone photonic crystal waveguides have been experimentally demonstrated to have lower optical propagation loss, high dispersion, and continuous delay tunability [14]. However, their intrinsic nonlinear group-delay spectrum limits the scope of their applications.

Chirped Bragg grating waveguides exhibit low propagation loss, wide operation bandwidth, continuous delay tuning, and compact footprints [16, 17]. Their tuning speed depends on the tunable laser and can reach the MHz level. Furthermore, the number of delay channels can be reduced by wavelength division multiplexing [4, 18] and channel-shared structures [19]. In the past several years, spiral and contra-directionally coupled Bragg grating waveguides with positive and negative dispersions have been fabricated, and multi-channel time-delay arrays have been developed based on these structures [20–23]. However, chirped Bragg gratings generally suffer from large GDE, which hinders their practical applications. The GDE originates, on one hand, from the ripples in the group delay spectra, which can be well suppressed by apodization [17, 20–23] and, on the other hand, from the nonlinear relation between the group delay and wavelength, which is induced by the nonlinear gradient of the mode effective index along the waveguide.

In this study, the width of the waveguide is nonlinearly corrected to solve the problem of the nonlinear delay spectrum of the contra-directionally coupled chirped Bragg grating waveguide. First, the nonlinear effect of grating apodization on the mode effective index is analyzed. Subsequently, the width of the waveguide is designed to have a nonlinear gradient to compensate for this nonlinear effect. Finally, a linear group delay spectrum is successfully obtained in the experiment.

2 Principle and design

Schematics of the contra-directionally coupled chirped Bragg grating waveguide are shown in Fig. 1. Conventional structure, as shown in Fig. 1a, consists of two tapered strip waveguides with widths ranging from w_1 and w_2 to $w_1+\Delta w$ and $w_2+\Delta w$, respectively. Bragg gratings with a period Λ, duty of 50%, and width w_a are introduced on the sidewall of the upper waveguide. To avoid bandwidth overlap between the contra-directionally coupling and back reflections, the width difference between the two waveguides must be large

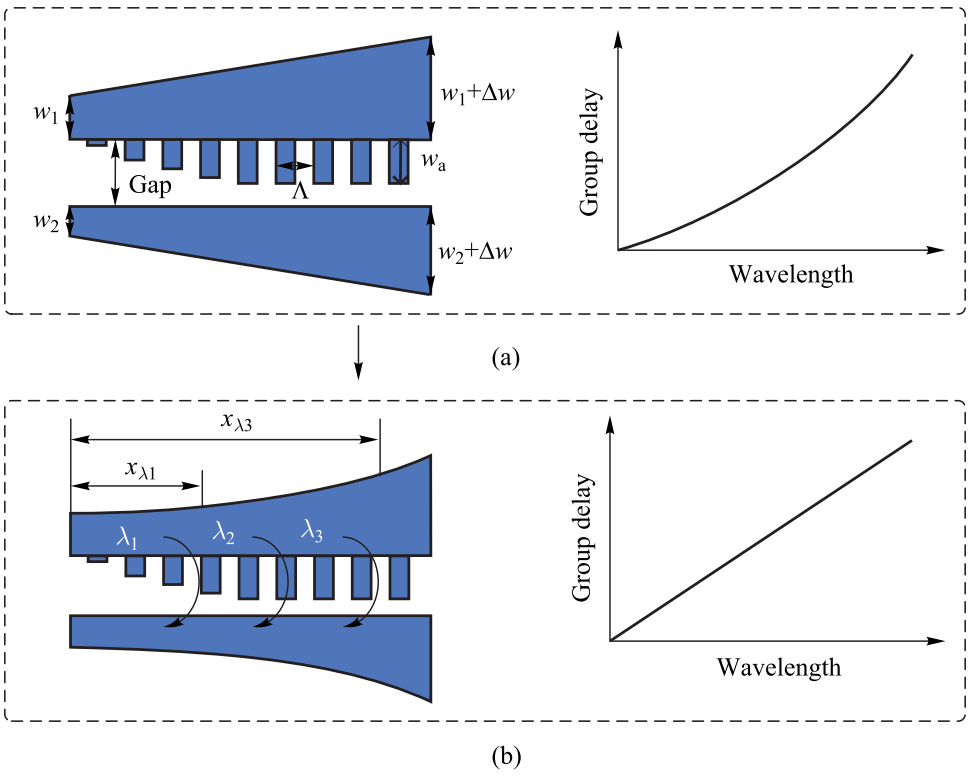

Fig. 1 Schematic diagrams of the contra-directionally coupled chirped Bragg grating waveguide and group delay spectra. **a** Conventional structure has linearly graded waveguide width and shows a nonlinear group delay spectrum, **b** proposed structure has corrected graded waveguide width and shows a linear group delay spectrum

enough [23]. The main structure parameters in this study are set as follows: $w_1 = 584$ nm, $w_2 = 484$ nm, $\Delta w = 20$ nm, gap = 200 nm, $\Lambda = 300$ nm, $w_a = 50$ nm, and the grating period number is 4800. To suppress the delay ripples, sinusoidal apodization of the gratings was applied over one-third of the entire grating length on the input side. The width of the apodized grating w_g can be expressed as follows:

$$w_g(x) = \begin{cases} w_a \cdot \sin[x \cdot (3/L) \cdot (\pi/2)], & x \le L/3, \\ w_a, & x > L/3, \end{cases} \quad (1)$$

where L is the whole length of the gratings; x is the location along the waveguide; w_a is the maximum grating width.

In the conventional design, the widths of tapered strip waveguides are set to increase linearly to achieve a linear increase in the mode effective index along the waveguide [21–23]. However, the grating apodization introduces a nonlinear change in the mode effective index, resulting in a nonlinear group delay spectrum. To obtain a linear group delay spectrum, we propose that the width of the tapered strip waveguide should be nonlinearly corrected to compensate for the effect of grating apodization on the mode effective index; the improved structure is shown in Fig. 1b. The design of the chirped Bragg grating waveguides with linear group delay is implemented by using the equations as follows:

$$\lambda_c = 2 \cdot n_{eff} \cdot \Lambda, \quad (2)$$

$$n_{eff} = (n_1 + n_2)/2, \quad (3)$$

$$n_{eff} = a \cdot x + n_{eff_0}, \quad (4)$$

$$\lambda_c = 2 \cdot \Lambda \cdot a \cdot x + 2 \cdot \Lambda \cdot n_{eff_0}, \quad (5)$$

$$l = 2 \cdot x = (\lambda_c - 2 \cdot \Lambda \cdot n_{eff_0})/(\Lambda \cdot a), \quad (6)$$

$$t = l/v_g = (\lambda_c - 2 \cdot \Lambda \cdot n_{eff_0})/(\Lambda \cdot a \cdot v_g), \quad (7)$$

where n_1, n_2, and n_{eff} are the mode effective indexes of upper and lower waveguides and coupled chirped Bragg grating waveguide composed of the upper and lower waveguides; λ_c is the central wavelength reflected by the chirped Bragg gratings; a and n_{eff_0} are constants; x is the location along the waveguide; l is the optical path length; t is the group delay; and v_g is the group velocity.

According to Eq. (2), λ_c changes with n_{eff} and Λ. For contra-directionally coupled chirped Bragg grating waveguides, n_{eff} is the average value of the mode effective indices of the upper and lower waveguides (Eq. (3)) [22, 23]. In this study, Λ is set as a constant, and n_{eff} is designed to increase linearly with x (Eq. (4)). Thus, λ_c also increases linearly with x (Eq. (5)). In Eq. (4), positive dispersion is obtained when a is positive; conversely, negative dispersion occurs when a is negative. As shown in Fig. 1b, light of different wavelengths is reflected at different positions in the waveguide, and the reflection position x_λ is proportional to the wavelength λ, according to Eq. (5). For the Bragg gratings, the optical path length l is twice of x_λ (Eq. (6)). Thus, the group delay can be calculated using Eq. (7). Supplementary Information: Fig. S1 shows the simulation results of v_g at the two ends of the contra-directionally coupled chirped Bragg grating waveguide. v_g at the two ends are approximately 7.13 at 1553 nm and 7.18 at 1562 nm with a variation of only ± 0.35%; therefore, v_g can be considered as a constant parameter. According to Eq. (7), the group delay, t, also increases linearly with the wavelength.

In the simulation of strip waveguides, it is found that the mode effective index does not linearly depend on the waveguide width in the large sweeping range of the waveguide width (Supplementary Information: Fig. S2a). However, the relationship between them tends to be linear within a small width range of 20 nm, as shown in Supplementary Information: Fig. S2b and S2c. Thus, the mode effective index of the coupled waveguide calculated using Eq. (3) is also almost linear with increasing width. For waveguides with linearly increasing widths, as shown in Fig. 2a, n_{eff} also increases almost linearly with the location along the waveguide (Fig. 2a). However, it tends to be nonlinear when apodized gratings are added to the upper waveguide (Fig. 2b). Thus, it is confirmed that the apodized grating can induce a nonlinear change of n_{eff} along the waveguide. For the mode effective index simulation in Fig. 2b, the effective widths of the two tapered waveguides, w_{up_eff} and w_{down_eff} are expressed as follows:

$$w_{up\_eff}(x) = w_1 + \beta \cdot w_g(x)/4 + \Delta w \cdot x/L, \quad (8)$$

$$w_{down\_eff}(x) = w_2 + \beta \cdot w_g(x)/4 + \Delta w \cdot x/L, \quad (9)$$

where the constant parameter β is set to 0.8. To obtain a linearly increasing n_{eff}, a linear increase in the effective widths of the two tapered waveguides is required. Thus, the real widths of the two tapered waveguides w_{up} and w_{down} should be nonlinearly corrected as follows:

$$w_{up}(x) = w_1 + (\beta \cdot w_a/4 + \Delta w) \cdot x/L - \beta \cdot w_g(x)/4, \quad (10)$$

$$w_{down}(x) = w_2 + (\beta \cdot w_a/4 + \Delta w) \cdot x/L - \beta \cdot w_g(x)/4. \quad (11)$$

After nonlinear correction of the waveguide width, the n_{eff} curve tends to be linear, as shown in Fig. 2c, indicating a successful design.

The proposed gratings waveguides are fabricated on a commercial silicon-on-insulator (SOI) wafer with a 250 nm

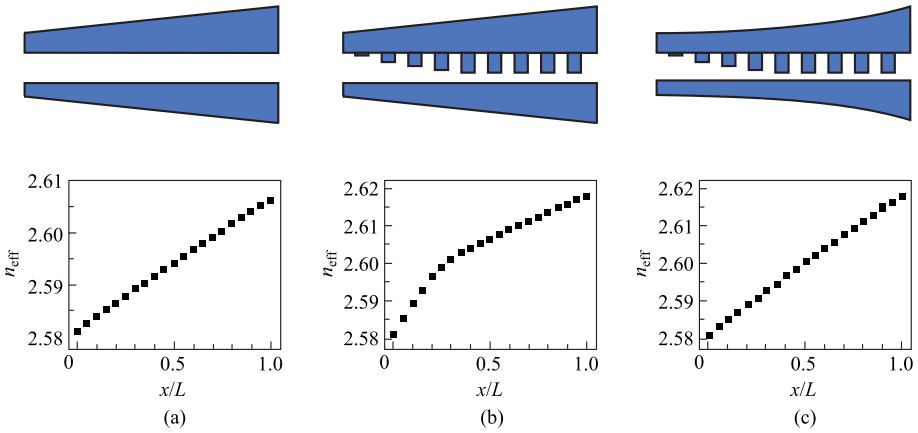

Fig. 2 Simulated mode effective index of the waveguides. **a** The waveguide width increases linearly from 484 to 504 nm for the upper one and 584–604 nm for the lower one; **b** the waveguides have linearly increased width with apodized grating, grating apodization follows Eq. (1) and the maximum w_a is 50 nm; **c** the waveguides have nonlinearly corrected width with apodized gratings

silicon layer and a 3 μm buried oxide layer. The waveguides on the top silicon layer are fabricated by electron beam lithography and silicon dry etching. A silicon dioxide layer is then deposited on the waveguide for encapsulation.

3 Results and discussion

The waveguides after nonlinear width correction are shown in Fig. 3a. According to Eq. (1), the width of the apodized gratings w_g increases sinusoidally, which induces a rapid increase in the effective widths of the two tapered waveguides w_{up_eff} and w_{down_eff}, according to Eqs. (8) and (9), resulting in an excessively rapid increase in n_{eff} (Fig. 2b). To compensate for this excessive increase in w_{up_eff} and w_{down_eff}, the real widths of the two tapered waveguides, w_{up} and w_{down}, need to be decreased slightly. As shown in Fig. 3b, when the grating width is 19 nm, w_{up} and w_{down} are 582.7 and 482.7 nm, respectively, which are smaller than the initial values of 584 and 484 nm, respectively. Figure 3c shows the SEM image of the waveguides in the apodization region. w_g, w_{up}, and w_{down} are 19, 582, and 482 nm,

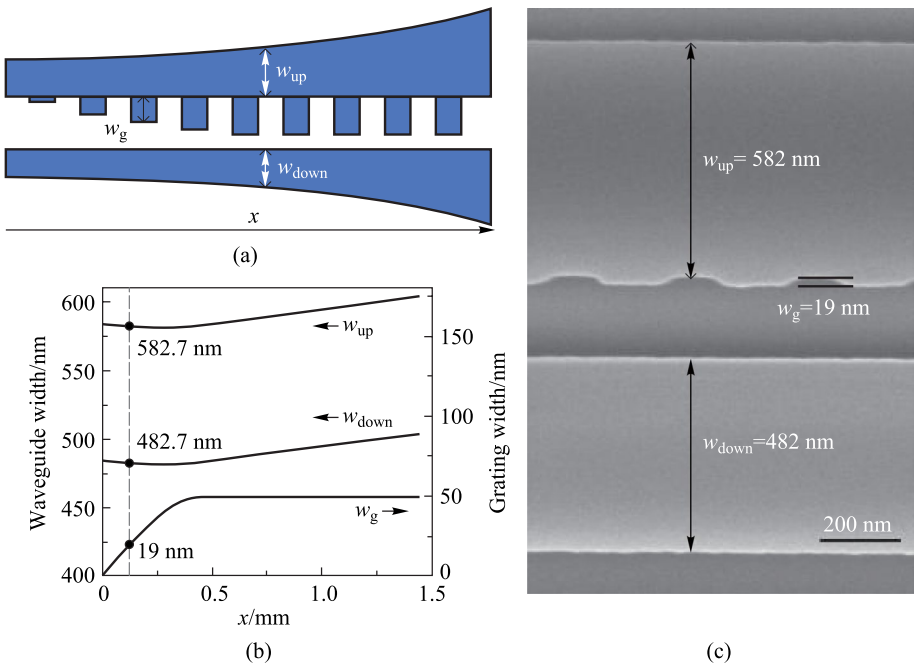

Fig. 3 Chirped Bragg gratings waveguide after width nonlinear correction: **a** schematic diagram, **b** variation of the simulated w_{up}, w_{down}, and w_g, and **c** SEM image

respectively and these values are consistent with those of the designed waveguide, as shown in Fig. 3b.

Figure 4a and b show the simulated transmission and group delay spectra of the grating waveguide with a linearly increasing width of the strip waveguide, and the corresponding waveguide structures and simulated n_{eff} are shown in Fig. 2b. The rapidly increasing n_{eff} at the narrow waveguide side shown in Fig. 2b leads to a shorter coupling length per wavelength space, which in turn results in a low transmission at the short wavelength side of the transmission spectrum in Fig. 4a, as well as a slowly increasing group delay at the short wavelength side of the group delay spectrum in Fig. 4b. When the widths of the strip waveguide are nonlinearly corrected, as shown in Fig. 2c, the transmission at the short wavelength side increases (Fig. 4c) compared to that shown in Fig. 4a, and the group delay curve becomes linear across the transmission spectrum (Fig. 4d).

The measurement setup for group delay is schematically shown in Fig. 5. A tunable laser is used to generate a light carrier, then a 10 GHz sinusoidal radio frequency (RF) signal is loaded on the light carrier through an intensity modulator (IM). The modulated signal is then injected into the fabricated contra-directionally coupled Bragg grating waveguides. Finally, the output signal is detected by a photodetector (PD) and analyzed by an oscilloscope (OSC). Due to the polarization dependence of IM and on-chip gratings

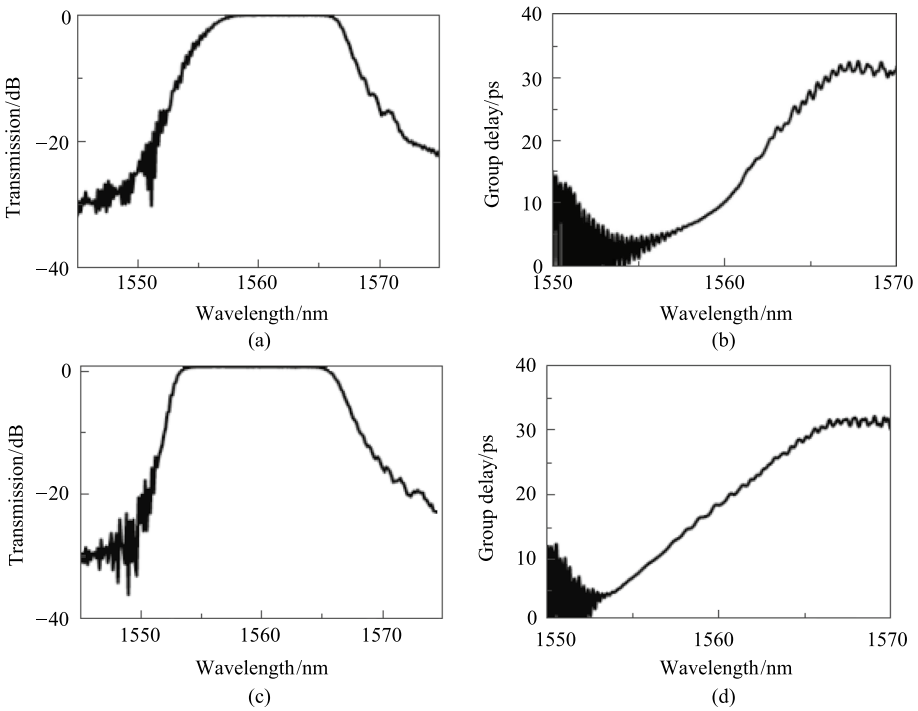

Fig. 4 Simulated transmission and group delay spectra of the contra-directionally coupled chirped Bragg gratings waveguides with linearly increasing waveguide width (**a** and **b**), and nonlinearly corrected waveguide width (**c** and **d**)

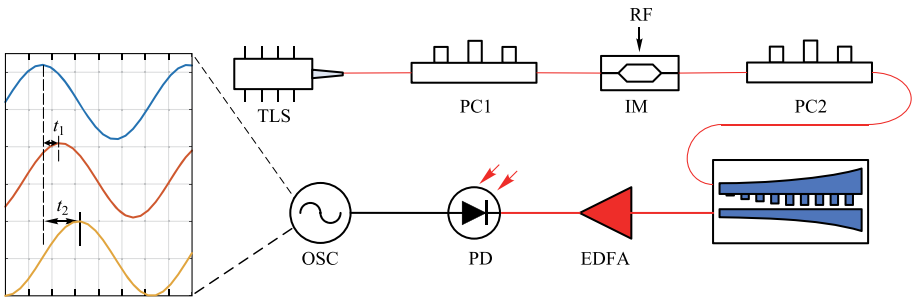

Fig. 5 Measurement setup for group delay. *TLS* tunable laser source, *PC* polarization controller, *RF* radio frequency source, *IM* intensity modulator, *EDFA* erbium doped fiber amplifier, *PD* photodetector, *OSC* oscilloscope

coupler, two polarization controllers (PCs) are placed before the IM and the chip respectively to maximize the coupling efficiency. When the input wavelength changes within the passband of the coupled Bragg grating waveguides, the detected waveforms will have different time delays. By obtaining the time delay at different wavelengths, the group delay lines can be calculated.

Figure 6 shows the measured transmission and group delay spectra of the grating waveguides with the structure shown in Fig. 2b and c. For both structures, the spectral bandwidth of the chirped Bragg grating waveguide is approximately 9 nm, the maximum group delay is approximately 30 ps, and the central wavelength is located at 1557.5 nm. The measurement results (Fig. 6a–d) agree well with the simulation results in Fig. 4a–d in terms of bandwidth and total group delay. The group delay line in Fig. 6b shows an upward bending trend, which is consistent with the simulated delay lines in Fig. 4b; this nonlinear bend produces a large GDE after linear fitting, where the GDE is calculated by the difference between the measured time delay and the linear fitted time delay. The measured average GDE is approximately ± 2 ps, which is approximately ± 7% of the total delay (Fig. 6e). In contrast, the group delay line in Fig. 6d is well matched linearly, and the measured average GDE is approximately ± 1 ps, which is approximately ± 4% of the total delay (Fig. 6f). Thus, it is proven that nonlinear correction of the waveguide width can effectively improve the linearity of the delay curve.

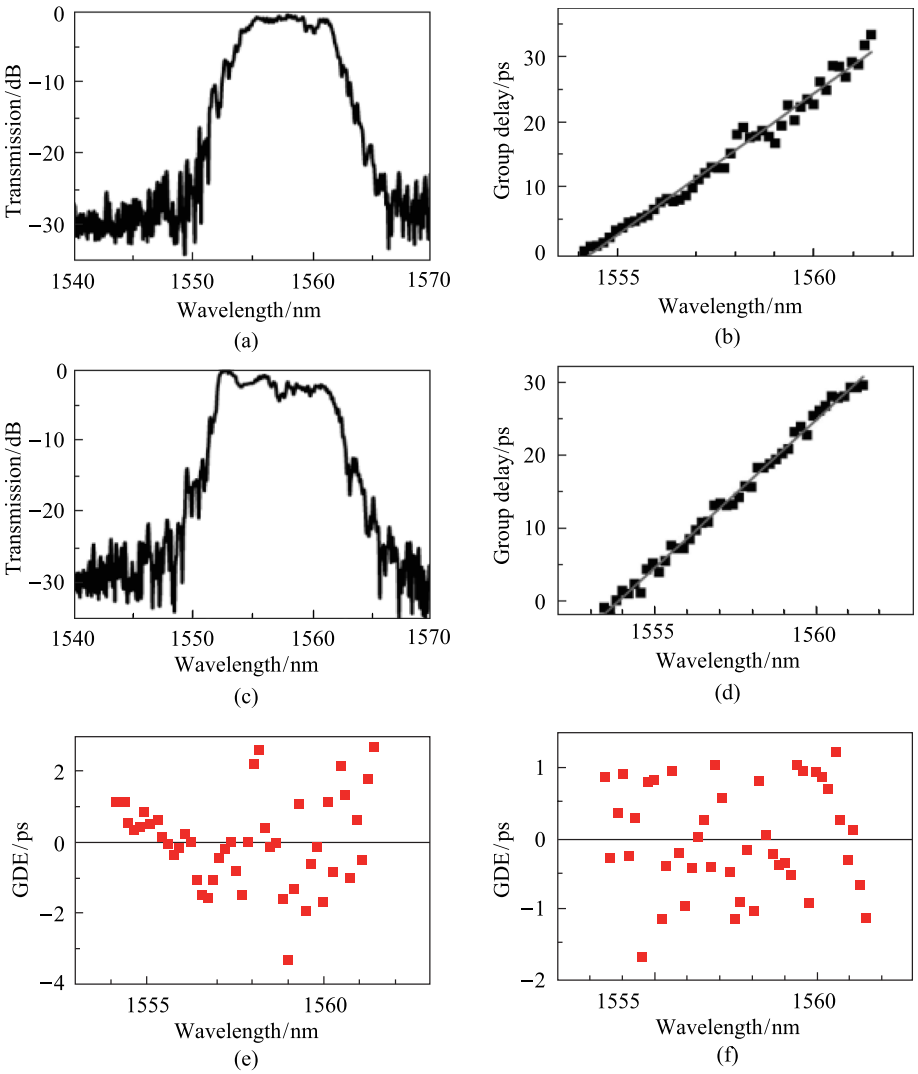

Fig. 6 Measured transmission, group delay, and GDE spectra of the contra-directionally coupled chirped Bragg grating waveguides with linearly increasing waveguide width (**a**, **b** and **e**), and nonlinearly corrected waveguide width (**c**, **d** and **f**)

4 Conclusions

This study is devoted to solving the problem of nonlinear delay spectrum of a contra-directionally coupled Bragg grating waveguide. Through the analysis of the mode effective index, it is found that grating apodization leads to a nonlinear gradient of the mode effective index along the waveguide, which then results in a nonlinear delay spectrum. To solve this problem, the width of the two strip waveguide in the coupled Bragg grating waveguides is nonlinearly corrected to compensate for the effect of the grating apodization on the mode effective index. As a result, a linear group delay spectrum is obtained in the experiment, and the GDE is halved compared the pre-correction case.

Supplementary Information The online version contains supplementary material available at https://doi.org/10.1007/s12200-023-00061-8.

Acknowledgements This work was supported by the key research and development program of Anhui province (202104a05020052, 2022a05020027), and open project program of Wuhan national laboratory for optoelectronics (2020WNL0KF005).

Author contributions XG designed the silicon photonic devices, YZ, CY, and SH participated in the device measurement, ZX, ZD, FZ, and JD participated in results analysis and manuscript preparation. All authors read and approved the final manuscript.

Availability of data and materials The data that support the findings of this study are available from the first author, upon reasonable request.

Declarations

Competing interests The authors declare that they have no competing interests.

References

1. Yang, H., Yun, B.: A six bit silicon nitride optical true time delay line for Ka-band phased array antenna. J. Phys. Conf. Ser. **1634**(1), 012173 (2020)
2. Jeong, J., Yom, I., Kim, J., Lee, W., Lee, C.A.: 6–18-GHz GaAs multifunction chip with 8-bit true time delay and 7-bit amplitude control. IEEE Trans. Microw. Theory Tech. **66**(5), 2220–2230 (2018)
3. Choo, G., Madsen, C.K., Palermo, S., Entesari, K.: Automatic monitor-based tuning of an RF silicon photonic 1×4 asymmetric binary tree true-time-delay beamforming network. J. Lightwave Technol. **36**(22), 5263–5275 (2018)
4. Ye, X., Zhang, F., Pan, S.: Compact optical true time delay beamformer for a 2D phased array antenna using tunable dispersive elements. Opt. Lett. **41**(17), 3956–3959 (2016)
5. Wang, C., Zhang, M., Chen, X., Bertrand, M., Shams-Ansari, A., Chandrasekhar, S., Winzer, P., Lončar, M.: Integrated lithium niobate electro-optic modulators operating at CMOS-compatible voltages. Nature **562**(7725), 101–104 (2018)
6. He, M., Xu, M., Ren, Y., Jian, J., Ruan, Z., Xu, Y., Gao, S., Sun, S., Wen, X., Zhou, L., Liu, L., Guo, C., Chen, H., Yu, S., Liu, L., Cai, X.: High-performance hybrid silicon and lithium niobate Mach-Zehnder modulators for 100 Gbit· s^{-1} and beyond. Nat. Photonics **13**(5), 359–364 (2019)
7. Lischke, S., Peczek, A., Morgan, J.S., Sun, K., Steckler, D., Yamamoto, Y., Korndörfer, F., Mai, C., Marschmeyer, S., Fraschke, M., Krüger, A., Beling, A., Zimmermann, L.: Ultra-fast germanium photodiode with 3-dB bandwidth of 265 GHz. Nat. Photonics **16**(3), 925–931 (2022)
8. Li, M., Zhu, N.: Recent advances in microwave photonics. Front. Optoelectron. **9**(2), 160–185 (2016)
9. Xie, J., Zhou, L., Li, Z., Wang, J., Chen, J.: Seven-bit reconfigurable optical true time delay line based on silicon integration. Opt. Express **22**(19), 22707–22715 (2014)
10. Wang, X., Zhou, L., Li, R., Xie, J., Lu, L., Wu, K., Chen, J.: Continuously tunable ultra-thin silicon waveguide optical delay line. Optica **4**(5), 507–515 (2017)
11. Song, L., Chen, T., Liu, W., Liu, H., Peng, Y., Yu, Z., Li, H., Shi, Y., Dai, D.: Toward calibration-free Mach-Zehnder switches for next-generation silicon photonics. Photon. Res. **10**(3), 793–801 (2022)
12. Xiang, C., Davenport, M.L., Khurgin, J.B., Morton, P.A., Bowers, J.E.: Low-loss continuously tunable optical true time delay based on Si_3N_4 ring resonators. IEEE J. Sel. Top. Quantum Electron. **24**(4), 5900109 (2018)
13. Lin, D., Xu, X., Zheng, P., Yang, H., Hu, G., Yun, B., Cui, Y.: A tunable optical delay line based on cascaded silicon nitride microrings for Ka-band beamforming. IEEE Photonics J. **11**(5), 5503210 (2019)
14. Chung, C., Xu, X., Wang, G., Pan, Z., Chen, R.T.: On-chip optical true time delay lines featuring one-dimensional fishbone photonic crystal waveguide. Appl. Phys. Lett. **112**(7), 071104 (2018)
15. Cassan, E., Roux, X.L., Caer, C., Hao, R., Bernier, D., Marris-Morini, D., Vivien, L.: Silicon slow light photonic crystals structures: present achievements and future trends. Front. Optoelectron. China **4**(3), 243–253 (2011)
16. Kaushal, S., Cheng, R., Ma, M., Mistry, A., Burla, M., Chrostowski, L., Azaña, J.: Optical signal processing based on silicon photonics waveguide Bragg gratings. Front Optoelectron. **11**(2), 163–188 (2018)
17. Du, Z., Xiang, C., Fu, T., Chen, M., Yang, S., Bowers, J.E., Chen, H.: Silicon nitride chirped spiral Bragg gratings with large group delay. APL Photonics **5**(10), 101302 (2020)
18. Ortega, B., Mora, J., Chulia, R.: Optical beamformer for 2-D phased array antenna with subarray partitioning capability. IEEE Photonics J. **8**(3), 6600509 (2016)
19. Gao, X., Zhu, Y., Chong, Y., Xu, Z., Mei, L., Cao, J., Zhang, F., Dong, J.: Integrated channel-shared optical true time delay line array based on gratings-assisted contradirectional couplers for phased array antennas. Proc. SPIE **11763**, 117633W (2021)
20. Sun, Y., Wang, D., Deng, C., Lu, M., Huang, L., Hu, G., Yun, B., Zhang, R., Li, M., Dong, J., Wang, A., Cui, Y.: Large group delay in silicon-on-insulator chirped spiral Bragg gratings waveguide. IEEE Photonics J. **13**(5), 5500205 (2021)

21. Shi, W., Veerasubramanian, V., Patel, D., Plant, D.V.: Tunable nanophotonic delay lines using linearly chirped contradirectional couplers with uniform Bragg gratings. Opt. Lett. **39**(3), 701–703 (2014)
22. Wang, X., Zhao, Y., Ding, Y., Xiao, S., Dong, J.: Tunable optical delay line based on integrated gratings-assisted contradirectional couplers. Photon. Res. **6**(9), 880–886 (2018)
23. Zhang, F., Dong, J., Zhu, Y., Gao, X., Zhang, X.: Integrated optical true time delay network based on gratings-assisted contradirectional couplers for phased array antennas. IEEE J. Sel. Top. Quantum Electron. **26**(5), 8302407 (2020)

Xudong Gao received his Ph.D. degree in Condensed Matter Physics from the University of Chinese Academy of Sciences, China in 2015. He is currently a senior engineer in Anhui Province Engineering Laboratory for Antennas and Microwave and East China Research Institute of Electronic Engineering, China. His current research interests include silicon photonics and optical control phase control matrix.

Zhenzhu Xu received her Ph.D. degree from South China University of Technology, China in 2019. From 2016 to 2019, she engaged research and development in the areas of nanotechnology and semiconductor devices. She is now working at East China Research Institute of Electronic Engineering, Hefei, China, focusing on the research of integrated optoelectronics, silicon photonics, and microwave photonic systems.

Yupeng Zhu received his Ph.D. degree from University of Science and Technology of China in 2017. He is now working at The 38th Research Institute of China Electronics Technology Group Corporation, focusing on silicon photonics and application of integrated optoelectronics in microwave systems.

Chengkun Yang received his Ph.D. degree in Optics from Nankai University, China, in 2019, and he is currently an engineer in Anhui Province Engineering Laboratory for Antennas and Microwave and East China Research Institute of Electronic Engineering, China. His research interests focus on microwave photonics and optoelectronic devices.

Shoubao Han received his Ph.D. degree in Optical Communication from Zhejiang University, China in 2019. He is currently working at East China Research Institute of Electronic Engineering, China. His main research focuses on silicon photonics and microwave photonic systems.

Zongming Duan received his bachelor's degree in Electronic Science and Technology from University of Electronic Science and Technology of China in 2005, and his master's degree in Electrical Engineering from Southeast University, China in 2013, and his Ph.D. degree in Electrical Engineering from University of Science and Technology of China in 2019. From 2005, he worked in East China Research Institute of Electronic Engineering (ECRIEE), China. He is now a RF/mm-wave integrated circuit expert and responsible for a RF integrated circuit design team in ECRIEE. He has authored or coauthored more than 30 academic papers and holds more than 10 patents. His current research interests include the design of RF/mm-wave/ Terahertz transceiver front ends and SoC in nanoscale CMOS, covering radar and communication.

Fan Zhang received his master's degree in Optical Engineering from Huazhong University of Science and Technology, China in 2021. He is currently working at InnoLight Technology (Suzhou) Ltd., China. His main research focuses on silicon photonics.

Jianji Dong received his Ph.D. degree in Optical Engineering from Huazhong University of Science and Technology (HUST), China in 2008. After that, he worked as postdoc at Cambridge University, UK till 2010. From March 2010, he returned to HUST and was promoted as a full professor in 2013. He is Professor of Wuhan National Laboratory for Optoelectronics (WNLO), HUST, China. His research interests include integrated microwave photonics, silicon photonics, and photonic computing. He has published more than 100 Journal papers. He has some special contribution to energy-efficient graphene silicon microheater, programmable temporal cloak, and complex spectrum analyzer of orbital angular momentum mode. He was honored the Fund of Excellent Youth Scholar by NSFC, China, and honored First award of Natural Science of Hubei Province. He is the Editorial Member of Scientific Reports, Associate Editor of IET Optoelectronics, and Executive Editor-in-Chief of Frontier of Optoelectronics. He is an IEEE Senior Member and OSA Member.